Nonadiabatic Dynamics of Photoexcited *cis*-Stilbene Using Ab Initio Multiple Spawning

Published as part of The Journal of Physical Chemistry virtual special issue "Peter J. Rossky Festschrift".

Hayley Weir, Monika Williams, Robert M. Parrish, Edward G. Hohenstein, and Todd J. Martínez*

ABSTRACT: The photochemistry of *cis*-stilbene proceeds through two pathways: *cis-trans* isomerization and ring closure to 4a,4b-dihydrophenanthrene (DHP). Despite serving for many decades as a model system for photoisomerization, the photodynamics of *cis*-stilbene is still not fully understood. We use *ab initio* multiple spawning on a SA-2-CASSCF(2,2) potential energy surface to simulate the nonadiabatic dynamics of isolated *cis*-stilbene. We find the cyclization (to DHP and *cis*-stilbene) and isomerization (to *trans*- and *cis*-stilbene) reaction coordinates to be orthogonal; branching between the two pathways is determined on the S_1 excited state within 150 fs of photoexcitation. Trajectory basis functions (TBFs) undergoing cyclization decay rapidly to the ground state in 250 fs, while TBFs moving along the isomerization coordinate remain on the excited state longer, with the majority decaying between 300 and 500 fs. We observe three avoided crossing regions in the dynamics: two along the isomerization coordinate (displaying pyramidalization and migration of an ethylenic hydrogen or phenyl group), and one DHP-like conical intersection along the cyclization coordinate. The isomeric form of the vibrationally hot photoproducts (as determined by measurement 2 ps after photoexcitation) is determined within less than 50 fs of decay to the ground state mediated by passage through a conical intersection. Excess vibrational energy of ground state *cis*- and *trans*-stilbene is channelled into phenyl torsions (with mostly opposing directionality). Our simulations are validated by direct comparison to experiment for the absorption spectrum, branching ratio of the three photoproducts (44:52:4 *cis*-stilbene:*trans*-stilbene:DHP), and excited state lifetime (520 ± 40 fs).

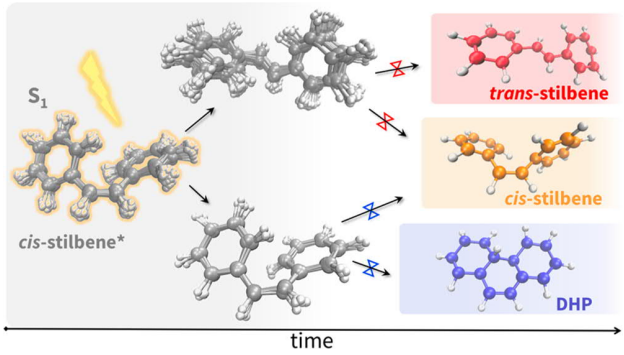

INTRODUCTION

Photochemistry offers a unique opportunity to manipulate molecules at an atomistic level with precision and control. Understanding these light-induced processes allows us to harness the properties of photoactive molecules for practical applications, such as creating more efficient solar cells, predicting the UV damage of DNA, developing fluorescent protein tags for cancer cell detection and exploring more efficient synthetic pathways for drug molecules.[1] Successful design of photoactive systems would benefit from a detailed understanding of fundamental photochemical mechanisms. One such mechanism is photoisomerization—rotation or inversion about a double bond upon excitation of the molecule with light. Photoisomerization is responsible for many key processes in both natural and synthetic devices, such as vision in the human eye, molecular motors, and optical data storage.[2] It may also contribute to fluorescence quenching in conjugated polymers such as poly(*p*-phenylene—vinylene) (PPV).[3−5]

Unsaturated hydrocarbons have long served as the subject of *cis*—*trans* photoisomerization studies due to their apparent mechanistic simplicity. However, over the past decades, the conventional one-dimensional model[6] of photoisomerization as torsion around the central carbon—carbon double bond has been shown to be too simplistic. For example, in the case of ethylene, the smallest unsaturated hydrocarbon, pyramidalization of one of the CH_2 groups (and intramolecular charge transfer) accompanies the double bond twist in the decay mechanism.[7−11] This departure from the conventional picture extends to photoisomerization of larger unsaturated hydrocarbons.[12,13]

Stilbene (1,2-diphenylethylene) shows remarkably similar photochemistry to ethylene and serves as a paradigm for photoisomerization. Stilbene exists in two isomers, *cis* and *trans*. Photoexcited *trans*-stilbene lives for tens of picoseconds

in the excited state due to trapping in a near-planar *trans* S_1 minimum. In contrast, the less stable *cis* isomer undergoes ultrafast decay within hundreds of femtoseconds.[14−19]

Following photoexcitation, *cis*-stilbene undergoes two competing photochemical reactions: photoisomerization to *trans*-stilbene and photocyclization to 4a,4b-dihydrophenanthrene (DHP), as illustrated in Scheme 1.[20] The cyclization of

Scheme 1. Photochemical Pathways of *cis*-Stilbene

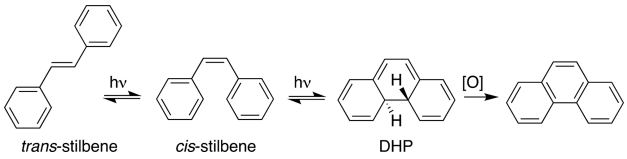

cis-stilbene to DHP adds an interesting dimension to the photodynamics: a simple example of a photoinduced ring-closure reaction, with potential applications in polycyclic drug-like molecule synthesis. Thus, the photochemistry of *cis*-stilbene is simultaneously an exemplar of both photoisomerization and photocyclization of a relatively large molecule.[21,22] We can expect that findings from the study of this prototypical molecule will likely extend to related molecules undergoing such fundamental photochemical reactions.

The stability of stilbene and its strong absorbance in the UV−visible region (corresponding to excitation to the optically bright $\pi \rightarrow \pi^*$ S_1 state) make it readily accessible for experimental studies.[23] The emergence of ultrafast time-resolved experiments in the past decades has seen *cis*-stilbene used as a prototype for probing femtosecond photoisomerization and testing new theoretical and experimental techniques. As a result, a plethora of experimental and theoretical data probing various aspects of *cis*-stilbene photochemistry is available, from early studies that determined coarse-grained observables such as branching ratios and energy differences, to emerging time dependent ultrafast gas phase studies. We start with a brief summary of previous investigations into *cis*-stilbene photochemistry.

Interest in *cis*-stilbene began when early experiments failed to observe any fluorescence (in contrast to the highly fluorescent *trans* isomer), indicating the presence of non-radiative decay pathways.[24] Moore et al. suggested that the major photochemical pathway was isomerization to *trans*-stilbene with a smaller portion undergoing cyclization to DHP, and a large portion returning to *cis*-stilbene.[20] Product branching ratios were later measured as 35% *trans*-stilbene, 55% *cis*-stilbene, and 10% DHP in hydrocarbon solvent at room temperature.[25]

Early experiments on *cis*-stilbene led to the hypothesis that decay to *trans*-stilbene was mediated by a "phantom state", p*, twisted about the central carbon−carbon double bond.[21,26,27] This phantom state is an S_1 minimum, located close to (but not at) an S_0/S_1 conical intersection (CI). In contrast to the *trans*-stilbene isomer, which gets trapped in a near-planar S_1 minimum after photoexcitation, there is little or no barrier to reach the phantom state on the excited state in *cis*-stilbene. Because of this, the excited state lifetime is very different in *trans* (≈80 ps) and *cis* (≈500 fs) isomers.[15,28] Although there has been some evidence for a shallow *cis*-like excited state minimum, its existence is still debated.[29,30]

Some of the first predictions of the atomistic mechanism came from a resonance Raman study, which suggested that the central double bond undergoes a 25° torsion in the first 20 fs.[31] However, in a study comparing many stilbene derivatives, Petek and co-workers suggested that 30% of the wavepacket instead followed the DHP cyclization coordinate after photoexcitation.[32]

Several early theoretical studies investigated the *cis*-stilbene S_1 potential energy surface (PES). A DHP-like CI was identified[33] with molecular-mechanics valence bond (MMVB) and a twisted CI along the isomerization coordinate was located[34] using state-averaged complete active space self-consistent field (SA-CASSCF). A comparative study of ethylene and stilbene elucidated the similarity of their respective CIs along the isomerization coordinate and noted that *cis*-stilbene isomerization was not one-dimensional but also involved a second coordinate: pyramidalization of one of the ethylenic carbon atoms.[8]

The emergence of time-resolved theoretical[35−38] and experimental[39−44] studies revealed an even more complicated photochemical mechanism. Time-resolved absorption spectroscopy suggested that a mixture of central double bond twisting, and carbon-phenyl torsion and in-plane bending initially takes place, followed by dephasing of the nuclear wavepacket.[40] Results from time-resolved Raman studies suggest that the isomerization is close to volume conserving.[41] There has been some controversy concerning the order of exponential decay for *cis*-stilbene in time-resolved fluorescence experiments. Tahara and co-workers interpreted their data in terms of biexponential decay in cyclohexane solvent, with time constants of 0.23 and 1.2 ps,[30] while Kovalenko and co-workers interpreted their data as monoexponential decay with a solvent dependent time constant (ranging from 0.21 to 0.75 ps).[45]

Many theoretical studies have considered the photodynamics of isolated *cis*-stilbene, focusing attention on the two lowest singlet electronic states. Time-dependent density functional theory (TDDFT),[46] spin−flip time-dependent density functional theory (SF-TDDFT),[47] restricted active space self-consistent field (RASSCF),[48] improved virtual orbital complete active space configuration interaction (IVO-CASCI),[49] and extended multiconfiguration quasi-degenerate perturbation theory (XMCQDPT2)[50] have recently been used to explore the PESs of isolated *cis*-stilbene in detail. Although these static studies provide valuable information about relevant stationary points on the ground and excited states, they cannot provide observables such as lifetimes and branching ratios for comparison to experiment or elucidation of reaction mechanisms. Recent attempts to incorporate dynamics have been carried out using DFT and SF-TDDFT.[51,52] Unfortunately, most DFT-based methods are incapable of describing the topology of S_0/S_1 conical intersections correctly and therefore are not suitable for nonadiabatic dynamics.[53] In principle, SF-TDDFT methods can treat the topology of S_0/S_1 CIs correctly, but these are often plagued with spin contamination that distorts the PESs. Consequently, the aforementioned SF-TDDFT dynamics studies were limited to the excited state and could not provide information about nonadiabatic transitions, excited state lifetimes, or photoproducts.

Despite extensive investigations, it is apparent that the internal conversion process in *cis*-stilbene is far from being understood in atomistic detail. New theoretical techniques for

modeling nonadiabatic dynamics and advances in computer hardware have made it possible to simulate the full nonadiabatic dynamics of a molecule of this size on the picosecond time scale. In this study, we couple graphical processing unit (GPU) accelerated state-averaged complete active space self-consistent field (SA-CASSCF)[54−56] electronic structure with *ab initio* multiple spawning (AIMS)[10,57] to simulate the full photodynamics of isolated *cis*-stilbene. This is the first dynamics simulation study of this molecule with a multireference electronic structure method encompassing a time scale that is sufficiently long to capture the complete nonadiabatic photochemical mechanism.

Our AIMS simulations provide a detailed account of the photochemical mechanism in *cis*-stilbene, including both *cis*-*trans* photoisomerization and ring closure to form DHP. We identify three minimum energy conical intersections (MECIs) accessed during the dynamics and their relation to photoproduct and reaction time scale, elucidate the role of phenyl torsion in the decay mechanism, describe the initial coherent motion of the wavepacket followed by its dephasing, and finally present a full mechanism for the photochemical reaction.

THEORETICAL METHODS

The accurate description of CIs involving the ground state (S_0) requires multireference electronic structure methods because of the exact degeneracy. The SA-CASSCF method[58] is able to capture these multireference effects ("static electron correlation") very effectively and thus has been a workhorse for studies of conical intersections in photochemistry.[10,57,59−61]

We employ SA-2-CASSCF(2,2) with the 6-31G* basis set to solve the electronic Schrödinger equation following $\pi \rightarrow \pi^*$ excitation. Previous work has demonstrated the reliability of SA-2-CASSCF(2,2) for stilbene through comparison to calculations including dynamic correlation with multireference perturbation theory (CASPT2).[8] However, extensive dynamics calculations on the requisite time scales were infeasible even with CASSCF because of computational expense. Our recent implementation[54] of SA-CASSCF on graphical processing units (GPUs) removes this bottleneck and enables multipicosecond time scale nonadiabatic dynamics for molecules of stilbene size (or even larger) with hundreds of initial conditions to address statistical convergence. We are therefore able to model *cis*-stilbene with a reliable description of the potential energy surfaces, including passage of the wavepacket through conical intersections. All SA-CASSCF and DFT calculations were performed with the TERACHEM quantum chemistry package.[62−64] MS-CASPT2 calculations were performed with the MOLPRO electronic structure package.[65]

We validate the chosen SA-CASSCF method by (1) comparison of critical point energies and geometries (including ground and excited state minima and conical intersections) to MS-CASPT2/SA-3-CASSCF(2,2)/6-31G* calculations including dynamic correlation effects and (2) direct comparison to experimental data such as the absorption spectrum, photoproduct branching ratio, and excited state lifetime. In accord with previous work, we find that the qualitative features of the PESs are in reasonable agreement between the two methods. Further discussion and comparison of electronic structure methods, including energy and geometry comparisons at critical points, are provided in the Supporting Information.

The absorption spectrum for isolated *cis*-stilbene is calculated by computing transition energies and oscillator strengths with SA-2-CASSCF(2,2)/6-31G* at 500 geometries sampled from the 0 K harmonic Wigner distribution, following previous work.[66−68] Lorentzian broadening with FWHM of 0.25 eV was used.

The photodynamics of isolated *cis*-stilbene is simulated using *ab initio* multiple spawning[10] (AIMS) with evaluation of SA-CASSCF potential energy surfaces, gradients, and nonadiabatic couplings as needed. AIMS is a semiclassical method used to model nonadiabatic nuclear dynamics that is compatible with "on-the-fly" evaluation of the electronic wave function through simultaneous solution of the electronic and nuclear Schrödinger equations. It approximates the exact molecular quantum dynamics by expanding the nuclear wavepacket in a basis of time-dependent frozen Gaussians, each of which propagates classically along a single adiabatic potential energy surface (PES). These frozen Gaussians are referred to as trajectory basis functions (TBFs). When a TBF approaches a region of strong nonadiabatic coupling with another electronic state, e.g., in regions close to a CI, a child TBF is "spawned" on the second state. The population transfer to the child TBF is determined through the solution of the time-dependent Schrödinger equation in the adaptive basis of TBFs. After the spawning event, when the TBFs have moved out of the coupling region, the parent and child TBFs continue along their respective adiabatic PESs until another electronic state crossing is detected, at which point the process repeats. Because the TBFs correspond to nuclear basis functions and therefore the matrix elements decay with separation between the TBFs, decoherence effects[69−73] appear automatically in AIMS. Therefore, there is no need for ad hoc corrections,[74,75] as in trajectory surface hopping.[76] AIMS has been previously applied to a number of other photoisomerization reactions.[11,12,77−79] For an in-depth discussion, the interested reader is directed to previous reviews.[57,80]

All AIMS dynamics simulations were carried out with the FMS90 program package (interfaced to TERACHEM) using an adaptive time-step scheme with an upper bound of 20 atomic time units (≈0.5 fs) and a total simulation time of 2 ps. Once TBFs on the ground state overlap negligibly with other TBFs in the simulation, they are terminated and restarted as independent adiabatic molecular dynamics trajectories using B3LYP/6-31G*. Our AIMS simulations begin with 100 TBFs whose initial positions and momenta are drawn from a 0 K harmonic Wigner distribution based on vibrational frequencies calculated with B3LYP/6-31G* at the B3LYP/6-31G* S_0 *cis*-stilbene minimum. These TBFs are promoted to the optically bright S_1 excited state and propagated in the independent first generation (IFG) approximation,[81] which assumes that phase coherence between initial conditions is negligible. The IFG approximation does retain interferences between TBFs that are spawned within any of the independent initial conditions.

In AIMS, the nuclear wave function is represented as a linear combination of TBFs that follow classical evolution on a specific adiabatic electronic state. In general, the analysis should therefore proceed by reconstruction of the time-evolving nuclear density matrix. In the IFG approximation, this implies incoherent summation over the density matrix generated by each initial condition. The density matrix for each initial condition is determined by coherent summation over the initial TBF and all the TBFs spawned thereafter. We use this analysis for the excited state population (and thus also the excited state lifetime). It can also be convenient to analyze the results in terms of the centroids of the TBFs—this analysis

is closer in spirit to what one would normally do in the context of TSH (although the amplitudes of the TBFs are complex and the different TBFs interfere with each other, so such analysis does not preclude possible differences in the dynamics). We use this classical analysis to succinctly describe the dynamics and photoisomerization mechanism and also to characterize the molecular geometries that are responsible for nonadiabatic transitions (exemplified by the "spawning geometries" where a parent TBF gives rise to a child TBF). This mixture of quantal and classical analysis allows us to obtain a detailed understanding of the simulated wavepacket. Bootstrapping[82] was used to calculate the statistical error of absolute values, such as photoproduct branching ratio and excited state lifetime, and the standard error was used for the error bars in the population decay.

RESULTS AND DISCUSSION

Experimental Comparison. We begin by validating our choice of theoretical method, SA-2-CASSCF(2,2), through comparison with three types of experimental data: absorption spectrum, photoproduct branching ratio, and excited state lifetime. Additional comparisons to benchmark multireference perturbation theory calculations can be found in the Supporting Information (Figure S1 and Table S1).

As seen in Figure 1, spectral shapes from SA-2-CASSCF-(2,2) and experiment are in good qualitative agreement. The

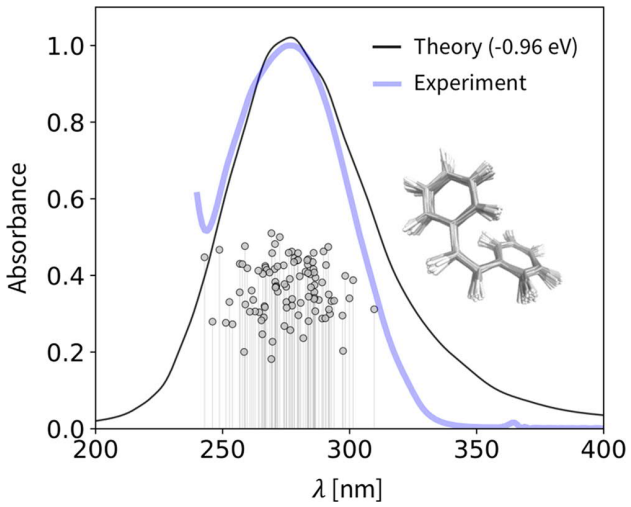

Figure 1. Comparison of SA-2-CASSCF(2,2) theoretical (black) and experimental (blue) absorption spectra. Initial conditions (gray ball and stick) are shown with height proportional to the oscillator strength, and molecular geometries are shown on the right. The theoretical data are red-shifted in energy by 0.96 eV to account for the absence of dynamic electron correlation in the CASSCF electronic structure method and convolved with a Lorentzian of width 0.25 eV. The experimental data correspond to solution measurements in hexane.[97]

absorption spectrum corresponds to the electronic transition from the $S_0 \rightarrow S_1$ state, a $\pi \rightarrow \pi^*$ transition. Figure 2 shows the HOMO and LUMO, elucidating the transfer of electron density from the central carbon−carbon π orbital to π bonds on the adjacent carbon pairs. This results in the introduction of a node between the ethylenic carbons, allowing for rotation about the central carbon−carbon bond and hence isomerization to *trans*-stilbene. One can also note the in-phase p-

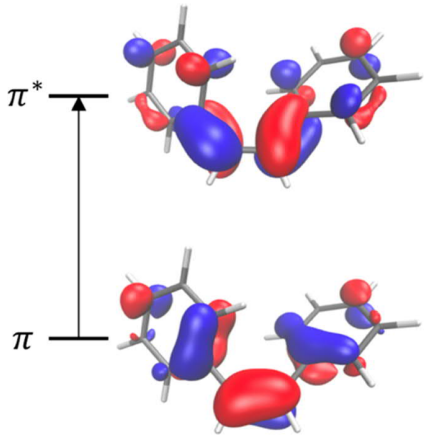

Figure 2. HOMO (π) and LUMO (π^*) of *cis*-stilbene at the Franck−Condon point calculated with SA-2-CASSCF(2,2) canonical orbitals.

orbitals on the phenyl rings in the LUMO, suggesting the possibility to form a new carbon−carbon σ bond between C_2 and $C_{2'}$ (labeling in Figure 3) and photocyclization to DHP.

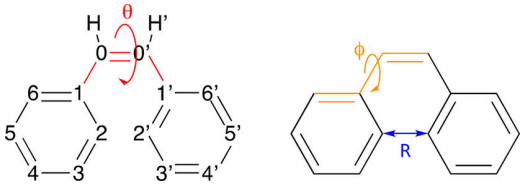

Figure 3. Coordinates in *cis*-stilbene nonadiabatic dynamics. Central $C_{1'}C_{0'}C_0C_1$ torsion angle, θ (red); phenyl $C_{0'}C_0C_1C_6$ torsion angle, ϕ (orange); DHP $C_2C_{2'}$ bond distance, R (blue).

Figure 3 shows the important coordinates in the photochemistry of *cis*-stilbene. We use these to categorize the three final ground state products (measured 2 ps after photoexcitation). TBFs where the centroid corresponds to $90° < \theta < 270°$ are labeled as *trans*-stilbene. Those with $R < 2$ Å are labeled as DHP, and all others are labeled as *cis*-stilbene. We validated this classification scheme by optimizing several of these geometries on S_0 (which all led to the labeled minima). With this classification, we obtain a branching ratio of 52.0 ± 3.6% *trans*-stilbene, 44.5 ± 3.7% *cis*-stilbene, and 3.5 ± 1.4% DHP. Here, we have assumed that the 7.1% of population that remains on S_1 at 2 ps will be distributed evenly between *cis*- and *trans*-stilbene since it resides close to the phantom state. This branching ratio is in line with recent experiments using transient absorption spectroscopy in acetonitrile with 318 nm excitation wavelength, which yielded 5% DHP.[83]

The excited state lifetime of *cis*-stilbene obtained from our dynamics simulations is 520 ± 40 fs. A time-resolved multiphoton ionization experiment measured a decay time of 320 fs for the ion current.[15] This should be considered a lower bound to the excited state lifetime, since the ionization propensity may decrease significantly when the molecule twists. Similar observations have been made for ethylene, where the decay of ion current was measured as 21 fs.[84,85] AIMS simulations reproduced the observed ion current signal for ethylene, but the excited state lifetime was found to be considerably longer (89 fs).[86] We plan on comparing our *cis*-stilbene simulation results to time-resolved photoelectron spectroscopy experiments in future work.

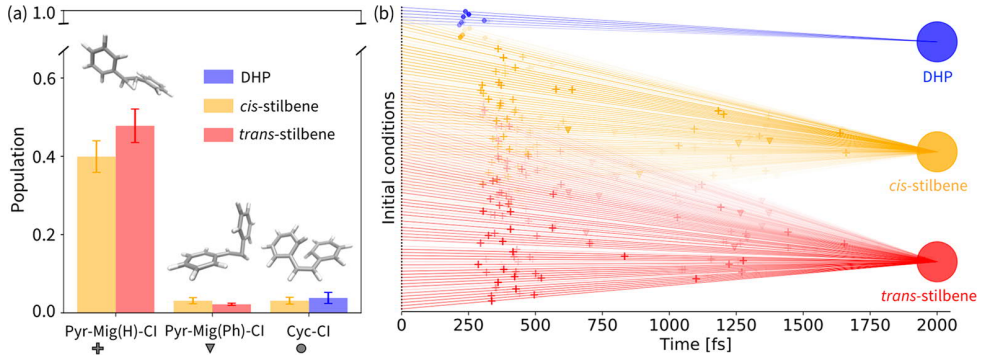

Figure 4. Summary of minimum energy conical intersection (MECI) results from AIMS dynamics. (a) Amount of population transfer corresponding to each MECI classified by final ground state product at 2 ps, and corresponding MECI geometries. Error bars were calculated from bootstrapping with 10 000 resamples. (b) Visualization of initial trajectories (black dots, t = 0 fs) and their final products (circles, t = 2 ps) of DHP (blue), *cis*-stilbene (red), and *trans*-stilbene (yellow). Minimum energy conical intersections (MECIs) are indicated at the time of spawning (marked by + (Pyr-Mig(H)-CI), ∇ (Pyr-Mig(Ph)-CI), ○ (Cyc-CI), and colored by the eventual product). The opacity of lines and markers are proportional to the population of the trajectory basis function associated with the product/MECI.

Photochemical Decay Pathways. Minimum energy conical intersections (MECIs) are often used as "signposts" when characterizing photochemical mechanisms, and quantifying the "reach" of an MECI gives insight into the weight that should be attributed to its importance in the mechanism. Figure 4a shows the three S_0/S_1 minimum energy conical intersection (MECIs) encountered during the dynamics simulations. Two of the MECIs exhibit pyramidalization of one ethylenic CHPh group, accompanied by either the migration of the pyramidalized hydrogen (Pyr-Mig(H)-CI) or phenyl group (Pyr-Mig(Ph)-CI). The third MECI resembles a cyclized product (Cyc-CI). Trajectories that decay via Cyc-CI lead to *cis*-stilbene and DHP only, and those that decay via Pyr-Mig(H)-CI and Pyr-Mig(Ph)-CI lead to *cis*- and *trans*-stilbene only, indicating two orthogonal reaction coordinates. Henceforth, we will refer to the former as the cyclization coordinate and the latter as the isomerization coordinate. The isomerization pathway (TBFs decaying via Pyr-Mig(H)-CI and Pyr-Mig(Ph)-CI) accounts for 93% of the wavepacket, leaving only 7% for the cyclization pathway (TBFs decaying via Cyc-CI).

As shown in Figure 4a, decay via Pyr-Mig(H)-CI is much more probable than via Pyr-Mig(Ph)-CI. This is likely due to the greater mobility of the smaller, lighter hydrogen atom relative to the bulky phenyl group, allowing for easier migration. This reasoning also rationalizes the late onset of the Pyr-Mig(Ph)-CI in comparison to the hydrogen migrated equivalent (see Figure 4b).

Following decay to the ground state via Pyr-Mig(H)-CI or Pyr-Mig(Ph)-CI, the simulations suggest that the wavepacket has a roughly equal probability of forming a *trans*- or *cis*-stilbene photoproduct, with a slight bias to *trans*-stilbene. Decay via Cyc-CI gives roughly an equal chance of forming DHP or *cis*-stilbene. It has been previously cited that 30% of the wavepacket initially follows the cyclization coordinate before splitting in a 2:1 ratio of DHP to *cis*-stilbene photoproducts.[32] However, this conclusion was drawn from the mechanistic similarity between *cis*-stilbene and its "locked" derivative. Since at early times our simulated wavepacket undergoes an ethylenic torsion for all trajectories, it is likely that the "locked" derivative also experiences this same torsion. As a result, the cited experimental data is not inconsistent with our simulations. Direct simulation of the various "locked" stilbene derivatives and comparison to *cis*-stilbene would be an interesting future direction that could shed further light on this.

Figure 4b illustrates that TBFs following the cyclization coordinate reach the intersection seam close to 220 fs, earlier than those that follow the isomerization coordinate, where the majority of population transfer to the ground state occurs between 300 and 500 fs. TBFs propagating along the isomerization pathway that remain in the excited state after the first 500 fs oscillate about the twisted S_1 minimum (the "phantom state"), gradually siphoning off population to S_0 until only a small fraction remain on S_1 at 2 ps.

As described previously, in AIMS dynamics a TBF spawns in a region of strong coupling between two electronic states, usually close to a CI. As a result, spawning may occur at a variety of energy gaps between the S_0 and S_1 PES surfaces. We define the population transfer efficiency for a spawning event as the population transferred to the child TBF after the spawning event divided by the population of the parent TBF prior to the spawning event. This should be distinguished from the absolute population transfer for a spawning event, which is defined as the population of the child TBF after the spawning event. The population of parent and child TBFs usually stabilize very quickly (within 15 fs) after a spawning event, so there is no practical ambiguity in these definitions. The distribution of population transfer efficiency and absolute population transfer at different energy gaps can give insight into the importance of the associated MECI in the dynamics.

A histogram of wavepacket population transfer at the spawning point at different energy gaps is plotted in Figure 5a, categorized by MECI. The majority of TBFs that decay close to Pyr-Mig(H)-CI are likely to have a small S_0/S_1 energy gap at the spawning event, with population transfer gradually dropping off as the energy difference increases. In contrast, Pyr-Mig(Ph)-CI and Cyc-CI appear to facilitate decay to S_0 at larger energy gaps. This indicates that the MECI is more important in the dynamics in the case of Pyr-Mig(H)-CI, and less so for Mig(Ph)-CI and Cyc-CI. Figure 5b illustrates that all three MECIs have a higher efficiency of population transfer close to the MECI, as you might expect. Therefore, the limiting factor for spawning close to the MECI is the ability to get there. As a result, the argument follows that it is harder to get close to the Mig(Ph)-CI and Cyc-CI and is easier to approach

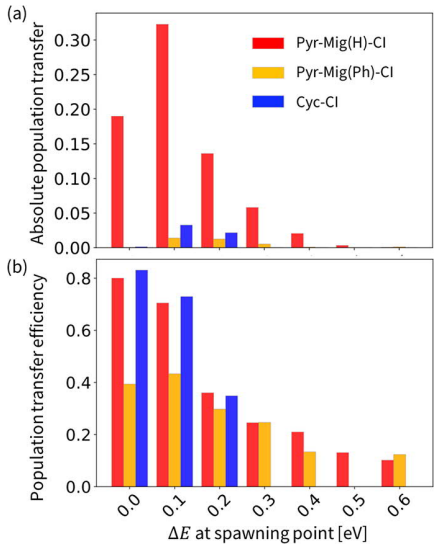

Figure 5. Absolute (top) and efficiency (bottom) population transfer through conical intersections at trajectory spawning point with the S_1/S_0 energy gap, ΔE. Absolute population transfer is defined as the total population transfer of the wavepacket through the CI at a given energy gap. Population transfer efficiency is defined as the average percentage population transferred to the child trajectory relative to the population of the parent at the point of spawning at a given energy gap. The populations are classified by minimum energy conical intersection (Cyc-CI, blue; Pyr-Mig(H)-CI, red; Pyr-Mig(Ph)-CI, orange).

the Pyr-Mig(H)-CI, giving insight into the possible shape of the PES around the MECIs.

Nonadiabatic Dynamics. The excited state population decay of the wavepacket (Figure 6) begins after a 200 fs delay while the wavepacket reaches the avoided crossing area. At this point, decay of TBFs following the cyclization coordinate occurs. Next, gradual decay of the portions of the wavepacket following the isomerization route proceeds from 300 to 500 fs, as seen in the MECI analysis, with the remaining 30% slowly tapering off until the vast majority of the wavepacket resides on the ground state at 2 ps.

An S_1 excited state lifetime of 520 ± 40 fs was obtained by observing the time at which the S_1 population has decayed to $1/e$. The wavepacket decay can be fitted to a biexponential decay, with time constants of 211 and 1026 fs for the fast and slow processes, respectively. The slow process encompasses the trapping of the wavepacket in the phantom state, and its gradual decay. Comparison between the biexponential and monoexponential decay, which gives a lifetime of 470 fs, as shown in Figure 6 suggests that the biexponential provides a better description of the wavepacket decay; however, the difference is not significant. As discussed earlier, both mono- and biexponential decay mechanisms have been suggested from time-resolved fluorescence experiments.

Rotation about the central C—C=C—C torsion angle (θ) is essential in the isomerization of *cis*-stilbene to *trans*-stilbene. The time evolution of this angle is plotted in Figure 7a. In the figure, all the TBFs are classified (as *cis*, *trans*, or DHP) at 2 ps according to the scheme discussed above and colored accordingly. There is a large (100°) coherent ethylenic torsion in the first 50 fs (depicted geometrically in Figure 8). Figure 7 reveals that the rapid torsion is due to the movement of only the ethylenic carbons, with the bulky phenyl rings remaining almost stationary during this initial twist. Following this, the

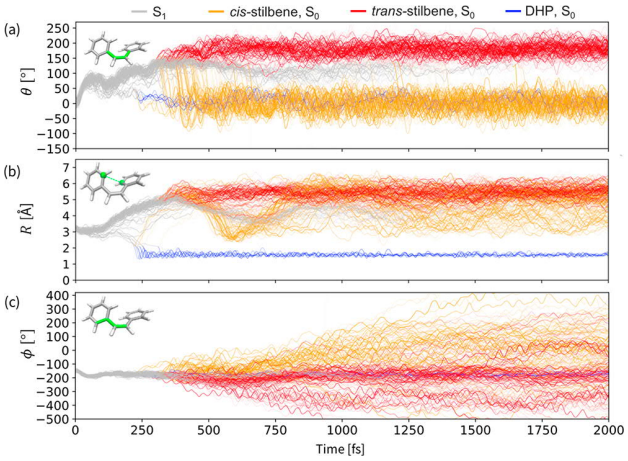

Figure 7. Geometry vs time plots along the AIMS trajectory as it decays from S_1 to S_0 after photoexcitation at $t = 0$ fs. (a) Central C—C=C–C torsion angle, θ. (b) C—C bond distance for DHP formation, R. (c) C=C—Ph torsion angle, ϕ. The line transparency is proportional to the trajectory amplitude and colored according to their product (DHP, blue; *cis*-stilbene, orange; *trans*-stilbene, red).

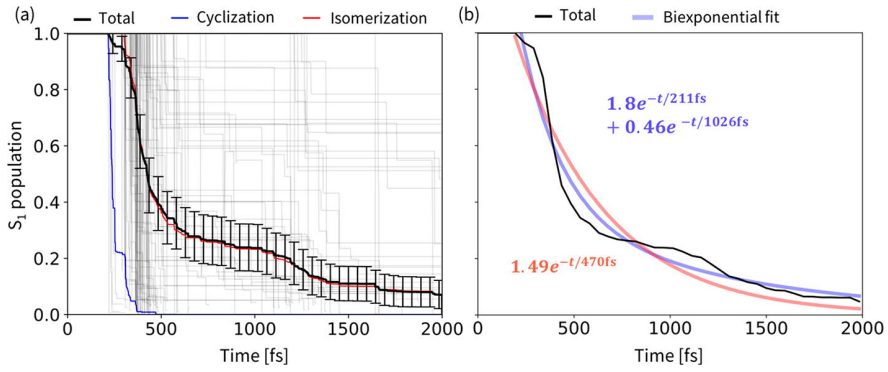

Figure 6. Decay of the S_1 population to S_0 with simulation time. (a) The average S_1 (thick black line) and individual trajectories (thin black lines) population decays are shown. The average population decays of the cyclization (blue) and isomerization (red) trajectories are also shown. Error bars are calculated using the standard error with a 95% confidence level. (b) Biexponential fit (thick blue) and monoexponentially fit (thick red) of the average total S_1 wavepacket (black). Biexponential lifetimes: 211 and 1026 fs. Monoexponential lifetime: 470 fs.

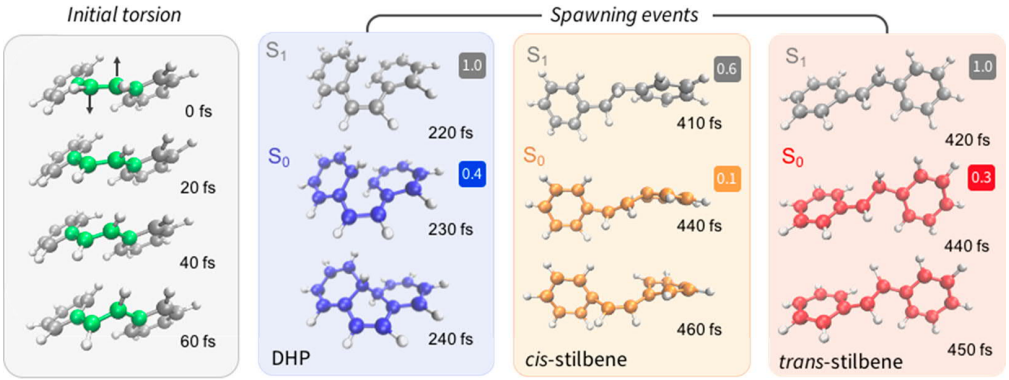

Figure 8. Representative examples of the time evolution of trajectory geometries at important events during the nonadiabatic dynamics. Panels from left to right: example of the torsion of the central dihedral angle in the first 60 fs of dynamics (gray background); example of spawning regions for DHP (blue background), *cis*-stilbene (orange background), and *trans*-stilbene (red background) from the excited state (gray molecular structure) to the ground state geometry (DHP, blue molecular structure; *cis*-stilbene, orange molecular structure; *trans*-stilbene, red molecular structure). Populations corresponding to TBFs are given in colored boxes. The time of spawning occurs between the color change from gray to blue/orange/red, demonstrating that within 10−50 fs after the spawning event the trajectory has formed a distorted version of the final photoproduct and remains in this same photoproduct until its measurement at 2 ps. This product formation in the spawning region applies to the majority of trajectories in the simulation.

central torsion of TBFs propagating along the isomerization coordinate oscillates toward 120° with a period of 100 fs, where the majority of population transfer occurs between 300 and 500 fs. TBFs that go on to form *trans*-stilbene continue to rotate to 180°, in contrast to those that form *cis*-stilbene, which "rebound" to a torsion angle of ∼0°. The ethylenic hydrogens are very hot following a spawning event in the case of *trans*-stilbene photoproducts, as illustrated in Figure S4, suggesting that they are an important reaction coordinate (reminiscent of the hydrogen out-of-plane or HOOP motion in photoisomerization of retinal protonated Schiff base[87−90]). TBFs following the cyclization coordinate oscillate about 0° after the initial cohesive torsion.

The key coordinate involved in the formation of DHP is the carbon−carbon distance corresponding to the newly formed bond, *R*. Figure 7b shows the evolution of this distance over time. The first 100 fs of the dynamics shows little motion in the CC bond distance, as the initial energy is almost exclusively channelled into the large initial ethylenic torsion. The next 100 fs, however, shows a sharp decrease in distance of the excited state wavepacket along the cyclization pathway (silver → blue), as the phenyl rings begin to approach each other. Note that the TBFs undergoing isomerization (silver → red), however, see a sharp increase in the bond distance as the phenyl rings twist away from each other. The excited state cyclizing TBFs then transfer population to S_0, at which point the ground state TBF can have two outcomes. A further decrease in CC distance leads to the DHP photoproduct, with the bond distance stabilizing around 1.5 Å. Alternatively, the rings repel each other and begin rotating, leading to the *cis*-stilbene photoproduct. The latter results in a rapid increase in *R* immediately after the spawn and energy transfer to low frequency oscillation phenyl torsions.

As alluded to earlier, our simulations show that excess energy on the ground state is transferred to phenyl torsion modes, ϕ, occurring immediately after decay to the ground state. Plotting the time evolution of this coordinate (Figure 7c) reveals a 50° dihedral rotation of the wavepacket between 0 and 50 fs, accompanying the central phenyl torsion. Ground state *trans*-stilbene products also exhibit phenyl rotations, along with the back and forth torsion of the central ethylenic carbons as the major relaxation mode. Interestingly, the rotations of the *cis*-stilbene and *trans*-stilbene products are largely unidirectional, with opposite directions adopted for each isomer.

One bond flip (OBF) and hula twist (HT) isomerization mechanisms have long been a topic of debate for many unsaturated organic molecules, including *cis*-stilbene.[42,91−94] Our simulations suggest a mostly OBF mechanism on S_1 from the increase in torsion angle with little in-plane bending of the C═CPh angle. However, the large amount of kinetic energy gained upon relaxation on S_1 leads to large amplitude motion that could be argued to bridge both OBF and HT type motions. Moreover, due to the phenyl rotations described above, a mixture of HT and OBF products are observed after decay to the ground state. This complicates the inference of photochemical pathways from experimental observations of product conformers. Mechanistic classification of *cis*-stilbene photochemistry as exclusively OBF or HT may be an oversimplification of a very hot molecule decaying via a complicated photochemical mechanism.

Analysis of the outlined geometric coordinates allows us to predict within 150 fs of photoexcitation whether a TBF will propagate along the photoisomerization or photocyclization pathway. As a result, we are able to do early time prediction of the photochemical coordinate (isomerization vs cyclization) and hence very early on distinguish TBFs that could go on to form *trans*-stilbene from those that could go on to form DHP. The final photoproduct of the TBF is formed in the spawning region; representative examples of such spawning events are displayed in Figure 8. Once the vibrationally hot form of the photoproduct has been formed immediately after the spawning event, it remains stable for the remainder of the simulation; i.e., we do not observe any interconversion between photoproducts on S_0 within the 2 ps simulation window. Such interconversion may of course occur on longer time scales (for example, DHP products undergoing ring-opening to form *cis*-stilbene).

Tahara and co-workers measured fluorescence lifetimes of 0.23 and 1.2 ps for *cis*-stilbene in solution.[30] Excited state SF-TDDFT dynamics suggested that these time scales correspond

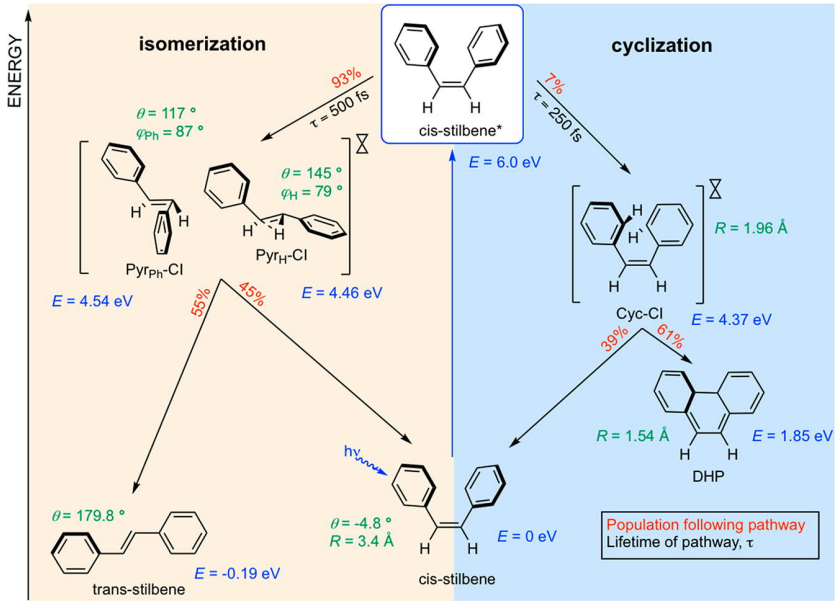

Figure 9. Summary of the photochemical decay mechanism of *cis*-stilbene following excitation to S_1. Population (red) and lifetime (black) associated with each pathway are given. Geometries are positioned at their relative SA-2-CASSCF(2,2) energies, *E*, (blue), with important geometric coordinates highlighted (green): central C—C=C–C torsion angle, θ; phenyl C=C—Ph torsion angle, ϕ; DHP C—C bond distance, *R*; hydrogen migration angle CCH, φ_H; phenyl migration angle CCPh, φ_{Ph}.

to the formation of *trans*-stilbene and DHP, respectively.[52] However, this could not be confirmed because the simulations did not encompass the nonadiabatic transitions and ground state dynamics. Our simulations show that the faster process corresponds to decay of DHP and *cis*-stilbene along the cyclization pathway, followed by rapid decay of *trans*- and *cis*-stilbene along the isomerization pathway and subsequently a slower decay of the trapped wavepacket in the phantom state (also along the isomerization coordinate). Our simulations predict excited state lifetime time constants of 0.21 and 1.0 ps, in good agreement with the experimental fluorescence lifetimes. Both the SF-TDDFT and AIMS/CASSCF studies agree that the early nuclear dynamics is responsible for the final branching and that the cyclization and isomerization coordinates compete with each other.

A summary of the overall nonadiabatic photochemical decay mechanism as described by AIMS dynamics on a SA-CASSCF(2,2) PES is shown in Figure 9. The lifetimes and yields of each key process in the reaction are highlighted, along with critical point geometries along the reaction coordinates and their associated energies. Comparison of the photochemical mechanism predicted by our AIMS dynamics largely agrees with the conclusions laid out in previous experimental and theoretical studies of *cis*-stilbene. For example, we observe that splitting of the wavepacket between the competing isomerization and cyclization pathways occurs very early on in the dynamics, and as one would expect from the assumed proximity of Cyc-CI to the FC point in comparison to the isomerization CIs, DHP is formed faster than *trans*-stilbene. The three minimum energy CIs that are encountered in the dynamics are consistent with those suggested in the SF-TDDFT dynamics study. We are able to confirm that the cyclization pathway leads to exclusively DHP and *cis*-stilbene and that the isomerization pathway leads exclusively to *trans*- and *cis*-stilbene, as seen in Figures 4 and 7. It has also become increasingly apparent that the ethylenic hydrogens play a central role in the photochemical mechanism, which is corroborated by our simulations: we see highly energetic movement of the hydrogens in the spawning region of the twisted, pyramidalized CIs when TBFs form *trans*-stilbene, in comparison to much less vigorous hydrogen movement from TBFs that form *cis*-stilbene, as detailed earlier and highlighted in Figure S4.

In addition to confirming accepted aspects of the photoisomerization mechanism, we can also access missing details since we are able to follow the wavepacket from the excited state, through the conical intersections, and onto the ground state. For example, our simulations predict that the stable photoproduct to be formed can be deduced within 50 fs of the nonadiabatic transition to the ground state, as illustrated in Figure 8. This indicates that the wavepacket splits between *trans*- and *cis*-stilbene and between DHP and *cis*-stilbene at the CI. Furthermore, hot ground state *cis*- and *trans*-stilbene are seen to channel their excess vibrational energy into primarily phenyl torsion, evidenced in Figure 7c.

Simulation of the full wavepacket dynamics for 2 ps allows us to also examine quantitative properties of the photochemistry, such as the photochemical branching ratio and lifetimes of mechanistic events. As discussed earlier, the excited state lifetime and the final product branching ratios of the AIMS trajectories are in reasonable agreement with experimental values. Our AIMS simulations indicate that the wavepacket experiences a large rapid ethylenic torsion in the first 50 fs along the isomerization pathway (Figure 8) after which the wavepacket bifurcates, with just ~10% "rebounding" and traveling toward the cyclization conical intersection, and ~90% toward the isomerization intersections. This large initial torsion is consistent with Myers and Mathies interpretation of their resonance Raman spectra,[31] in spite of the later suggestion that the wavepacket initially follows the cyclization coordinate.[32]

Lastly, our nonadiabatic dynamics simulations suggest that the excited state isomerization pathway of isolated *cis*-stilbene follows a primarily "one bond flip" (OBF) mechanism, in contrast to recent proposals[42] for a "hula-twist" (HT) pathway. It is noted, however, that the coordinates involved in distinguishing between OBF and HT involve the ethylenic hydrogen atoms, which, as we have seen, are highly energetic and therefore can make the distinction rather difficult. Moreover, photochemical mechanisms may involve further rearrangements on the ground state (for example, the twisting of the phenyl rings on the ground state we observed), making it potentially troublesome to infer the pathway from regiochemistry of the final products.

Representative TBFs demonstrating the geometrical behavior of the four major pathways in *cis*-stilbene photochemistry (isomerization to *trans*- and *cis*-stilbene, and cyclization to DHP and *cis*-stilbene) are presented as supplemental movies.

■ CONCLUSIONS

In this study, we employed *ab initio* multiple spawning with SA-CASSCF to elucidate the photochemical reaction mechanism for *cis*-stilbene. The simulations provide a detailed picture of the decay of the wavepacket from S_1 to S_0, as summarized in Figure 9. Following a rapid initial ethylenic torsion, the wavepacket bifurcates between the orthogonal photoisomerization and photocyclization reaction coordinates. The appearance of ground state DHP (and *cis*-stilbene) from the part of the wavepacket that evolves along the cyclization coordinate occurs in the first 300 fs after passing through Cyc-CI. The remainder of the wavepacket, which evolves along the isomerization coordinate, decays to ground state *trans*- (and *cis*-) stilbene 0.3−2 ps after photoexcitation, via Pyr-Mig(H)-CI and Pyr-Mig(Ph)-CI. A small portion of the wavepacket experiences trapping in the S_1 twisted geometry, i.e., the phantom state. Phenyl rotations play an important role in the dissipation of energy during the hot ground state dynamics of *cis*- and *trans*-stilbene. Predicted excited state lifetimes and photoproduct branching ratios are largely in agreement with previous experimental findings, validating the simulation results.

Understanding the wavepacket decay of *cis*-stilbene allows for the systematic design of experiments that achieve a desired outcome, for example, altering the photoproduct branching ratio or changing the rate of the dynamics. The early wavepacket bifurcation seen in this study suggests that manipulation of the PES early in the dynamics, through the use of substituents, environment, or electric field, is more important than later in the dynamics if one wishes to control the ratio of isomerization vs cyclization. Knowledge of the dynamics of the wavepacket as it passes through the avoided crossing regions also allows for the possibility of mechanism manipulation that may not be evident with a static study. Moreover, since *cis*-stilbene is the parent to a vast number of derivative molecules, and arguably a prototype for *all* photoisomerization reactions, understanding its photodynamics and designing routes to steer its decay mechanism are likely applicable far beyond the scope of this single molecule study. An example of this lies in the importance of the ethylenic hydrogens in the photoisomerization mechanism, which could well govern the final photoproduct branching ratio. The simulations presented in this study suggest that the energetic movement of these atoms through the CI during the formation of *trans*-stilbene may be impeded if replaced with a heavier or bulkier alternative. This has potential to yield a greater portion of *cis*-stilbene, a concept that could well extended to alternative photoisomerizing molecules.

The results from these dynamics simulations can be directly linked to future ultrafast time-dependent pump−probe experiments, such as time-resolved photoelectron spectroscopy (TRPES) and ultrafast electron diffraction (UED). The signals from such experiments may then be decomposed and assigned. UED is well suited for tracking the nuclear wavepacket,[95] particularly the formation of the new carbon−carbon bond of the DHP photoproduct. Our simulations predict a rising signal corresponding to the new carbon−carbon bond (at 1.8 Å) from 200 fs onward. In contrast, TRPES maps the time-resolved electronic behavior of the wavepacket, which can provide information about the transitions between different electronic states in addition to probing nuclear motion.[13,96] The simulations presented in this paper will provide a template for interpretation of such UED and TRPES experiments in the future.

■ AUTHOR INFORMATION

Corresponding Author

Todd J. Martínez − *Department of Chemistry and The PULSE Institute, Stanford University, Stanford, California 94305, United States; SLAC National Accelerator Laboratory, Menlo Park, California 94025, United States;* orcid.org/0000-0002-4798-8947; Email: toddmtz@stanford.edu

Authors

Hayley Weir − *Department of Chemistry and The PULSE Institute, Stanford University, Stanford, California 94305, United States; SLAC National Accelerator Laboratory, Menlo Park, California 94025, United States;* orcid.org/0000-0002-1039-327X

Monika Williams − *Department of Chemistry and The PULSE Institute, Stanford University, Stanford, California 94305, United States; SLAC National Accelerator Laboratory, Menlo Park, California 94025, United States;* orcid.org/0000-0003-2292-6501

Robert M. Parrish − *Department of Chemistry and The PULSE Institute, Stanford University, Stanford, California 94305, United States; SLAC National Accelerator Laboratory, Menlo Park, California 94025, United States;* orcid.org/0000-0002-2406-4741

Edward G. Hohenstein − *Department of Chemistry and The PULSE Institute, Stanford University, Stanford, California 94305, United States; SLAC National Accelerator Laboratory, Menlo Park, California 94025, United States;* orcid.org/0000-0002-2119-2959

Notes

The authors declare no competing financial interest.

■ ACKNOWLEDGMENTS

This work was supported by the AMOS program of the U.S. Department of Energy, Office of Science, Basic Energy Sciences, Chemical Sciences, and Biosciences Division and by the Department of Energy, Laboratory Directed Research and Development program at SLAC National Accelerator Laboratory, under contract DE-AC02-76SF00515.

■ REFERENCES

(1) Garavelli, M. Computational Organic Photochemistry: Strategy, Achievements and Perspectives. *Theor. Chem. Acc.* **2006**, *116*, 87−105.

(2) Dugave, C.; Demange, L. Cis− Trans Isomerization of Organic Molecules and Biomolecules: Implications and Applications. *Chem. Rev.* **2003**, *103*, 2475−2532.

(3) Bedard-Hearn, M. J.; Sterpone, F.; Rossky, P. J. Nonadiabatic Simulations of Exciton Dissociation in Poly-P-Phenylenevinylene Oligomers. *J. Phys. Chem. A* **2010**, *114*, 7661−7670.

(4) Sterpone, F.; Bedard-Hearn, M. J.; Rossky, P. J. Nonadiabatic Mixed Quantum-Classical Dynamic Simulation of Pi-Stacked Oligophenylenevinylenes. *J. Phys. Chem. A* **2009**, *113*, 3427−3430.

(5) Sterpone, F.; Rossky, P. J. Molecular Modeling and Simulation of Conjugated Polymer Oligomers: Ground and Excited State Chain Dynamics of Ppv in the Gas Phase. *J. Phys. Chem. B* **2008**, *112*, 4983−4993.

(6) Turro, N. J. *Modern Molecular Photochemistry*; University Science: Sausalito, CA, 1991.

(7) Ben-Nun, M; Martınez, T. J Photodynamics of Ethylene: Ab Initio Studies of Conical Intersections. *Chem. Phys.* **2000**, *259*, 237−248.

(8) Quenneville, J.; Martinez, T. J. Ab Initio Study of Cis− Trans Photoisomerization in Stilbene and Ethylene. *J. Phys. Chem. A* **2003**, *107*, 829−837.

(9) Quenneville, J.; Ben-Nun, M.; Martınez, T. J. Photochemistry from First Principles—Advances and Future Prospects. *J. Photochem. Photobiol., A* **2001**, *144*, 229−235.

(10) Ben-Nun, M.; Quenneville, J.; Martinez, T. J. Ab Initio Multiple Spawning: Photochemistry from First Principles Quantum Molecular Dynamics. *J. Phys. Chem. A* **2000**, *104*, 5161−5175.

(11) Ben-Nun, M.; Martınez, T. J. Ab Initio Molecular Dynamics Study of Cis−Trans Photoisomerization in Ethylene. *Chem. Phys. Lett.* **1998**, *298*, 57−65.

(12) Levine, B. G.; Martínez, T. J. Ab Initio Multiple Spawning Dynamics of Excited Butadiene: Role of Charge Transfer. *J. Phys. Chem. A* **2009**, *113*, 12815−12824.

(13) Glover, W. J.; Mori, T.; Schuurman, M. S.; Boguslavskiy, A. E.; Schalk, O.; Stolow, A.; Martinez, T. J. Excited State Non-Adiabatic Dynamics of the Smallest Polyene, Trans 1,3-Butadiene. Ii. Ab Initio Multiple Spawning Simulations. *J. Chem. Phys.* **2018**, *148*, 164303.

(14) Doany, F.; Hochstrasser, R.; Greene, B.; Millard, R. Femtosecond-Resolved Ground-State Recovery of Cis-Stilbene in Solution. *Chem. Phys. Lett.* **1985**, *118*, 1−5.

(15) Greene, B.; Farrow, R. Subpicosecond Time Resolved Multiphoton Ionization: Excited State Dynamics of Cis-Stilbene under Collision Free Conditions. *J. Chem. Phys.* **1983**, *78*, 3336−3338.

(16) Todd, D. C.; Jean, J. M.; Rosenthal, S. J.; Ruggiero, A. J.; Yang, D.; Fleming, G. R. Fluorescence Upconversion Study of Cis-Stilbene Isomerization. *J. Chem. Phys.* **1990**, *93*, 8658−8668.

(17) Todd, D. C.; Fleming, G. R. Cis-Stilbene Isomerization: Temperature Dependence and the Role of Mechanical Friction. *J. Chem. Phys.* **1993**, *98*, 269−279.

(18) Sension, R. J.; Repinec, S. T.; Szarka, A. Z.; Hochstrasser, R. M. Femtosecond Laser Studies of the Cis-Stilbene Photoisomerization Reactions. *J. Chem. Phys.* **1993**, *98*, 6291−6315.

(19) Greene, B.; Hochstrasser, R.; Weisman, R. Photoproperties of Isolated Cis and Trans Stilbene Molecules. *Chem. Phys.* **1980**, *48*, 289−298.

(20) Moore, W. M.; Morgan, D. D.; Stermitz, F. R. The Photochemical Conversion of Stilbene to Phenanthrene. The Nature of the Intermediate. *J. Am. Chem. Soc.* **1963**, *85*, 829−830.

(21) Waldeck, D. H. Photoisomerization Dynamics of Stilbenes. *Chem. Rev.* **1991**, *91*, 415−436.

(22) Abourashed, E. A. Review of Stilbenes: Applications in Chemistry, Life Sciences and Materials Sciencestilbenes: Applications in Chemistry, Life Sciences and Materials Science. By Gertz Likhtenshtein. Wiley-Vch, Weinheim, Germany. 2009. 360 Pp. $224 Hardcover. Isbn 978−3-527−32388−3. *J. Nat. Prod.* **2017**, *80*, 577−577.

(23) Gegiou, D.; Muszkat, K.; Fischer, E. Temperature Dependence of Photoisomerization. V. Effect of Substituents on the Photoisomerization of Stilbenes and Azobenzenes. *J. Am. Chem. Soc.* **1968**, *90*, 3907−3918.

(24) Lewis, G. N.; Magel, T. T.; Lipkin, D. The Absorption and Re-Emission of Light by Cis-and Trans-Stilbenes and the Efficiency of Their Photochemical Isomerization. *J. Am. Chem. Soc.* **1940**, *62*, 2973−2980.

(25) Muszkat, K.; Fischer, E. Structure, Spectra, Photochemistry, and Thermal Reactions of the 4a, 4b-Dihydrophenanthrenes. *J. Chem. Soc. B* **1967**, 662−678.

(26) Saltiel, J. Perdeuteriostilbene. The Role of Phantom States in the Cis-Trans Photoisomerization of Stilbenes. *J. Am. Chem. Soc.* **1967**, *89*, 1036−1037.

(27) Orlandi, G.; Siebrand, W. Model for the Direct Photo-Isomerization of Stilbene. *Chem. Phys. Lett.* **1975**, *30*, 352−354.

(28) Abrash, S.; Repinec, S.; Hochstrasser, R. M. The Viscosity Dependence and Reaction Coordinate for Isomerization of Cis-Stilbene. *J. Chem. Phys.* **1990**, *93*, 1041−1053.

(29) Saltiel, J.; Waller, A. S.; Sears, D. F., Jr The Temperature and Medium Dependencies of Cis-Stilbene Fluorescence. The Energetics of Twisting in the Lowest Excited Singlet State. *J. Am. Chem. Soc.* **1993**, *115*, 2453−2465.

(30) Nakamura, T.; Takeuchi, S.; Taketsugu, T.; Tahara, T. Femtosecond Fluorescence Study of the Reaction Pathways and Nature of the Reactive S1 State of Cis-Stilbene. *Phys. Chem. Chem. Phys.* **2012**, *14*, 6225−6232.

(31) Myers, A. B.; Mathies, R. A. Excited-State Torsional Dynamics of Cis-Stilbene from Resonance Raman Intensities. *J. Chem. Phys.* **1984**, *81*, 1552−1558.

(32) Petek, H.; Yoshihara, K.; Fujiwara, Y.; Lin, Z.; Penn, J. H.; Frederick, J. H. Is the Nonradiative Decay of S1 Cis-Stilbene Due to the Dihydrophenanthrene Isomerization Channel? Suggestive Evidence from Photophysical Measurements on 1, 2-Diphenylcycloalkenes. *J. Phys. Chem.* **1990**, *94*, 7539−7543.

(33) Bearpark, M. J.; Bernardi, F.; Clifford, S.; Olivucci, M.; Robb, M. A.; Vreven, T. Cooperating Rings in Cis-Stilbene Lead to an S0/S1 Conical Intersection. *J. Phys. Chem. A* **1997**, *101*, 3841−3847.

(34) Amatatsu, Y. Ab Initio Study on the Electronic Structures of Stilbene at the Conical Intersection. *Chem. Phys. Lett.* **1999**, *314*, 364−368.

(35) Berweger, C. D.; van Gunsteren, W. F.; Müller-Plathe, F. Molecular Dynamics Simulation with an Ab Initio Potential Energy Function and Finite Element Interpolation: The Photoisomerization of Cis-Stilbene in Solution. *J. Chem. Phys.* **1998**, *108*, 8773−8781.

(36) Dou, Y.; Allen, R. E. Another Important Coordinate in the Photoisomerization of Cis-Stilbene. *Chem. Phys. Lett.* **2003**, *378*, 323−329.

(37) Dou, Y.; Allen, R. E. Detailed Dynamics of a Complex Photochemical Reaction: Cis−Trans Photoisomerization of Stilbene. *J. Chem. Phys.* **2003**, *119*, 10658−10666.
(38) Dou, Y.; Allen, R. E. Dynamics of the Photocyclization Ofcis-Stilbene to Dihydrophenanthrene. *J. Mod. Opt.* **2004**, *51*, 2485−2491.
(39) Baumert, T.; Frohnmeyer, T.; Kiefer, B.; Niklaus, P.; Strehle, M.; Gerber, G.; Zewail, A. H. Femtosecond Transition State Dynamics of Cis -Stilbene. *Appl. Phys. B: Lasers Opt.* **2001**, *72*, 105−108.
(40) Ishii, K.; Takeuchi, S.; Tahara, T. A 40-Fs Time-Resolved Absorption Study on Cis-Stilbene in Solution: Observation of Wavepacket Motion on the Reactive Excited State. *Chem. Phys. Lett.* **2004**, *398*, 400−406.
(41) Takeuchi, S.; Ruhman, S.; Tsuneda, T.; Chiba, M.; Taketsugu, T.; Tahara, T. Spectroscopic Tracking of Structural Evolution in Ultrafast Stilbene Photoisomerization. *Science* **2008**, *322*, 1073−1077.
(42) Fuß, W.; Kosmidis, C.; Schmid, W. E.; Trushin, S. A. The Photochemical Cis−Trans Isomerization of Free Stilbene Molecules Follows a Hula-Twist Pathway. *Angew. Chem., Int. Ed.* **2004**, *43*, 4178−4182.
(43) Quick, M.; Dobryakov, A. L.; Ioffe, I. N.; Granovsky, A. A.; Kovalenko, S. A.; Ernsting, N. P. Perpendicular State of an Electronically Excited Stilbene: Observation by Femtosecond-Stimulated Raman Spectroscopy. *J. Phys. Chem. Lett.* **2016**, *7*, 4047−4052.
(44) Harabuchi, Y.; Yamamoto, R.; Maeda, S.; Takeuchi, S.; Tahara, T.; Taketsugu, T. Ab Initio Molecular Dynamics Study of the Photoreaction of 1, 1′-Dimethylstilbene Upon S0→ S1 Excitation. *J. Phys. Chem. A* **2016**, *120*, 8804−8812.
(45) Sajadi, M.; Dobryakov, A. L.; Garbin, E.; Ernsting, N. P.; Kovalenko, S. A. Time-Resolved Fluorescence Spectra of Cis-Stilbene in Hexane and Acetonitrile. *Chem. Phys. Lett.* **2010**, *489*, 44−47.
(46) Improta, R.; Santoro, F. Excited-State Behavior of Trans and Cis Isomers of Stilbene and Stiff Stilbene: A Td-Dft Study. *J. Phys. Chem. A* **2005**, *109*, 10058−10067.
(47) Minezawa, N.; Gordon, M. S. Photoisomerization of Stilbene: A Spin-Flip Density Functional Theory Approach. *J. Phys. Chem. A* **2011**, *115*, 7901−7911.
(48) Tomasello, G.; Garavelli, M.; Orlandi, G. Tracking the Stilbene Photoisomerization in the S(1) State Using Rasscf. *Phys. Chem. Chem. Phys.* **2013**, *15*, 19763−19773.
(49) Chaudhuri, R. K.; Freed, K. F.; Chattopadhyay, S.; Mahapatra, U. S. Theoretical Studies of the Ground and Excited State Structures of Stilbene. *J. Phys. Chem. A* **2013**, *117*, 9424−9434.
(50) Ioffe, I. N.; Granovsky, A. A. Photoisomerization of Stilbene: The Detailed Xmcqdpt2 Treatment. *J. Chem. Theory Comput.* **2013**, *9*, 4973−4990.
(51) Neukirch, A. J.; Shamberger, L. C.; Abad, E.; Haycock, B. J.; Wang, H.; Ortega, J.; Prezhdo, O. V.; Lewis, J. P. Nonadiabatic Ensemble Simulations of Cis-Stilbene and Cis-Azobenzene Photoisomerization. *J. Chem. Theory Comput.* **2014**, *10*, 14−23.
(52) Harabuchi, Y.; Keipert, K.; Zahariev, F.; Taketsugu, T.; Gordon, M. S. Dynamics Simulations with Spin-Flip Time-Dependent Density Functional Theory: Photoisomerization and Photocyclization Mechanisms of Cis-Stilbene in Pipi* States. *J. Phys. Chem. A* **2014**, *118*, 11987−11998.
(53) Levine, B. G.; Ko, C.; Quenneville, J.; MartÍnez, T. J. Conical Intersections and Double Excitations in Time-Dependent Density Functional Theory. *Mol. Phys.* **2006**, *104*, 1039−1051.
(54) Snyder, J. W., Jr.; Fales, B. S.; Hohenstein, E. G.; Levine, B. G.; Martinez, T. J. A Direct-Compatible Formulation of the Coupled Perturbed Complete Active Space Self-Consistent Field Equations on Graphical Processing Units. *J. Chem. Phys.* **2017**, *146*, 174113.
(55) Snyder, J. W., Jr; Hohenstein, E. G.; Luehr, N.; Martínez, T. J. An Atomic Orbital-Based Formulation of Analytical Gradients and Nonadiabatic Coupling Vector Elements for the State-Averaged Complete Active Space Self-Consistent Field Method on Graphical Processing Units. *J. Chem. Phys.* **2015**, *143*, 154107.
(56) Hohenstein, E. G.; Luehr, N.; Ufimtsev, I. S.; Martínez, T. J. An Atomic Orbital-Based Formulation of the Complete Active Space Self-Consistent Field Method on Graphical Processing Units. *J. Chem. Phys.* **2015**, *142*, 224103.
(57) Curchod, B. F. E.; Martinez, T. J. Ab Initio Nonadiabatic Quantum Molecular Dynamics. *Chem. Rev.* **2018**, *118*, 3305−3336.
(58) Roos, B. O. The Complete Active Space Self-Consistent Field Method and Its Applications in Electronic Structure Calculations. *Adv. Chem. Phys.* **2007**, *69*, 399−445.
(59) Gozem, S.; Luk, H. L.; Schapiro, I.; Olivucci, M. Theory and Simulation of the Ultrafast Double-Bond Isomerization of Biological Choromophores. *Chem. Rev.* **2017**, *117*, 13502−13565.
(60) Virshup, A. M.; Punwong, C.; Pogorelov, T. V.; Lindquist, B. A.; Ko, C.; Martinez, T. J. Photodynamics in Complex Environments: Ab Initio Multiple Spawning Quantum Mechanical/Molecular Mechanical Dynamics. *J. Phys. Chem. B* **2009**, *113*, 3280−3291.
(61) Garavelli, M.; Bernardi, F.; Olivucci, M.; Vreven, T.; Klein, S.; Celani, P.; Robb, M. A. Potential-Energy Surfaces for Ultrafast Photochemistry: Static and Dynamic Aspects. *Faraday Discuss.* **1998**, *110*, 51−70.
(62) Ufimtsev, I. S.; Martinez, T. J. Quantum Chemistry on Graphical Processing Units. 1. Strategies for Two-Electron Integral Evaluation. *J. Chem. Theory Comput.* **2008**, *4*, 222−231.
(63) Ufimtsev, I. S.; Martinez, T. J. Quantum Chemistry on Graphical Processing Units. 2. Direct Self-Consistent-Field Implementation. *J. Chem. Theory Comput.* **2009**, *5*, 1004−1015.
(64) Ufimtsev, I. S.; Martinez, T. J. Quantum Chemistry on Graphical Processing Units. 3. Analytical Energy Gradients, Geometry Optimization, and First Principles Molecular Dynamics. *J. Chem. Theory Comput.* **2009**, *5*, 2619−2628.
(65) Werner, H.-J.; Knowles, P. J.; Knizia, G.; Manby, F. R.; Schütz, M. Molpro: A General-Purpose Quantum Chemistry Program Package. *WIRes: Comp. Mol. Sci.* **2012**, *2*, 242−253.
(66) Bergsma, J. P.; Berens, P. H.; Wilson, K. R.; Fredkin, D. R.; Heller, E. J. Electronic Spectra from Molecular Dynamics: A Simple Approach. *J. Phys. Chem.* **1984**, *88*, 612−619.
(67) Barbatti, M.; Aquino, A. J.; Lischka, H. The Uv Absorption of Nucleobases: Semi-Classical Ab Initio Spectra Simulations. *Phys. Chem. Chem. Phys.* **2010**, *12*, 4959−4967.
(68) Curchod, B. F.; Sisto, A.; Martinez, T. J. Ab Initio Multiple Spawning Photochemical Dynamics of Dmabn Using Gpus. *J. Phys. Chem. A* **2017**, *121*, 265−276.
(69) Prezhdo, O. V.; Rossky, P. J. Evaluation of Quantum Transition Rates from Quantum-Classical Molecular Dynamics Simulations. *J. Chem. Phys.* **1997**, *107*, 5863−5878.
(70) Bittner, E. R.; Rossky, P. J. Quantum Decoherence in Mixed Quantum-Classical Systems: Nonadiabatic Processes. *J. Chem. Phys.* **1995**, *103*, 8130−8143.
(71) Prezhdo, O. V.; Rossky, P. J. Relationship between Quantum Decoherence Times and Solvation Dynamics in Condensed Phase Chemical Systems. *Phys. Rev. Lett.* **1998**, *81*, 5294.
(72) Bittner, E. R.; Rossky, P. J. Decoherent Histories and Nonadiabatic Quantum Molecular Dynamics Simulations. *J. Chem. Phys.* **1997**, *107*, 8611.
(73) Neria, E.; Nitzan, A. Semiclassical Evaluation of Nonadiaabtic Rates in Condensed Phases. *J. Chem. Phys.* **1993**, *99*, 1109.
(74) Granucci, G.; Persico, M. Critical Appraisal of the Fewest Switches Algorithm for Surface Hopping. *J. Chem. Phys.* **2007**, *126*, 134114.
(75) Subotnik, J. E.; Jain, A.; Landry, B.; Petit, A.; Ouyang, W. Understanding the Surface Hopping View of Electronic Transitions and Decoherence. *Annu. Rev. Phys. Chem.* **2016**, *67*, 387−417.
(76) Tully, J. C. Molecular Dynamics with Electronic Transitions. *J. Chem. Phys.* **1990**, *93*, 1061−1071.
(77) Martinez, T. J. Insights for Light-Driven Molecular Devices from Ab Initio Multiple Spawning Excited-State Dynamics of Organic and Biological Chromophores. *Acc. Chem. Res.* **2006**, *39*, 119−126.
(78) Ko, C.; Virshup, A. M.; Martínez, T. J. Electrostatic Control of Photoisomerization in the Photoactive Yellow Protein Chromophore:

Ab Initio Multiple Spawning Dynamics. *Chem. Phys. Lett.* **2008**, *460*, 272−277.
(79) Kim, J.; Tao, H.; Martinez, T. J.; Bucksbaum, P. Ab Initio Multiple Spawning on Laser-Dressed States: A Study of 1,3-Cyclohexadiene Photoisomerization Via Light-Induced Conical Intersections. *J. Phys. B: At., Mol. Opt. Phys.* **2015**, *48*, 164003.
(80) Mignolet, B.; Curchod, B. F. E. A Walk through the Approximations of Ab Initio Multiple Spawning. *J. Chem. Phys.* **2018**, *148*, 134110.
(81) Hack, M. D.; Wensmann, A. M.; Truhlar, D. G.; Ben-Nun, M.; Martınez, T. J. Comparison of Full Multiple Spawning, Trajectory Surface Hopping, and Converged Quantum Mechanics for Electronically Nonadiabatic Dynamics. *J. Chem. Phys.* **2001**, *115*, 1172−1186.
(82) Efron, B.; Tibshirani, R. J. *An Introduction to the Bootstrap*; Taylor and Francis: Boca Raton, FL, 1994.
(83) Kovalenko, S. A.; Dobryakov, A. L.; Ioffe, I.; Ernsting, N. P. Evidence for the Phantom State in Photoinduced Cis−Trans Isomerization of Stilbene. *Chem. Phys. Lett.* **2010**, *493*, 255−258.
(84) Farmanara, P.; Stert, V.; Radloff, W. Ultrafast Internal Conversion and Fragmentation in Electronically Excited C2h4 and C2h3cl Molecules. *Chem. Phys. Lett.* **1998**, *288*, 518−522.
(85) Kosma, K.; Trushin, S. A.; Fuss, W.; Schmid, W. E. Ultrafast Dynamics and Coherent Oscillations in Ethylene and Ethylene-D4 Excited at 162 Nm. *J. Phys. Chem. A* **2008**, *112*, 7514−7529.
(86) Tao, H.; Allison, T. K.; Wright, T. W.; Stooke, A. M.; Khurmi, C.; van Tilborg, J.; Liu, Y.; Falcone, R. W.; Belkacem, A.; Martinez, T. J. Ultrafast Internal Conversion in Ethylene. I. The Excited State Lifetime. *J. Chem. Phys.* **2011**, *134*, 244306.
(87) Kukura, P.; McCamant, D. W.; Yoon, S.; Wandschneider, D. B.; Mathies, R. A. Structural Observation of the Primary Isomerization in Vision with Femtosecond-Stimulated Raman. *Science* **2005**, *310*, 1006−1009.
(88) Schapiro, I.; Ryazantsev, M. N.; Frutos, L. M.; Ferre, N.; Lindh, R.; Olivucci, M. The Ultrafast Photoisomerizations of Rhodopsin and Bathorhodopsin Are Modulated by Bond Length Alternaiton and Hoop Driven Electronic Effects. *J. Am. Chem. Soc.* **2011**, *133*, 3354−3364.
(89) Liang, R.; Liu, F.; Martinez, T. J. Nonadiabatic Photodynamics of Retinal Protonated Schiff Base in Channelrhodopsin 2. *J. Phys. Chem. Lett.* **2019**, *10*, 2862−2868.
(90) Yu, J. K.; Liang, R.; Liu, F.; Martinez, T. J. First-Principles Characterization of the Elusive I Fluorescent State and the Structural Evolution of Retinal Protonated Schiff Base in Bacteriorhodopsin. *J. Am. Chem. Soc.* **2019**, *141*, 18193−18203.
(91) Liu, R. S.; Hammond, G. S. The Case of Medium-Dependent Dual Mechanisms for Photoisomerization: One-Bond-Flip and Hula-Twist. *Proc. Natl. Acad. Sci. U. S. A.* **2000**, *97*, 11153−11158.
(92) Liu, R. S. Photoisomerization by Hula-Twist: A Fundamental Supramolecular Photochemical Reaction. *Acc. Chem. Res.* **2001**, *34*, 555−562.
(93) Yang, L.-Y.; Harigai, M.; Imamoto, Y.; Kataoka, M.; Ho, T.-I.; Andrioukhina, E.; Federova, O.; Shevyakov, S.; Liu, R. S. Stilbene Analogs in Hula-Twist Photoisomerization. *Photochem. Photobio. Sci.* **2006**, *5*, 874−882.
(94) Lei, Y.; Yu, L.; Zhou, B.; Zhu, C.; Wen, Z.; Lin, S. H. Landscapes of Four-Enantiomer Conical Intersections for Photoisomerization of Stilbene: Casscf Calculation. *J. Phys. Chem. A* **2014**, *118*, 9021−9031.
(95) Wolf, T. J. A.; Sanchez, D. M.; Yang, J.; Parrish, R. M.; Nunes, J. P. F.; Centurion, M.; Coffee, R.; Cryan, J. P.; Guhr, M.; Hegazy, K.; Kirrander, A.; Li, R. K.; Ruddock, J.; Shen, X.; Vecchione, T.; Weathersby, S. P.; Weber, P. M.; Wilkin, K.; Yong, H.; Zheng, Q.; Wang, X. J.; Minitti, M. P.; Martinez, T. J. The Photochemical Ring-Opening of 1,3-Cyclohexadiene Imaged by Ultrafast Electron Diffraction. *Nat. Chem.* **2019**, *11*, 504−509.
(96) Boguslavskiy, A. E.; Schalk, O.; Gador, N.; Glover, W. J.; Mori, T.; Schultz, T.; Schuurman, M. S.; Martinez, T. J.; Stolow, A. Excited State Non-Adiabatic Dynamics of the Smallest Polyene, Trans 1,3-Butadiene. I. Time-Resolved Photoelectron-Photoion Coincidence Spectroscopy. *J. Chem. Phys.* **2018**, *148*, 164302.
(97) Taniguchi, M.; Lindsey, J. S. Database of Absorption and Fluorescence Spectra of> 300 Common Compounds for Use in Photochem Cad. *Photochem. Photobiol.* **2018**, *94*, 290−327.